Broadening effects and ergodicity in deep level photothermal spectroscopy of defect states in semi-insulating GaAs: A combined temperature-, pulse-rate-, and time-domain study of defect state kinetics

Jun Xia and Andreas Mandelis[a)]
Department of Mechanical and Industrial Engineering, Center for Advanced Diffusion-Wave Technologies (CADIFT), University of Toronto, Toronto, Ontario M5S 3G8, Canada

(Received 23 November 2008; accepted 14 April 2009; published online 28 May 2009)

The technique of deep level photothermal spectroscopy (DLPTS) is extended to the low temperature region in order to cover several defect states in semi-insulating GaAs. Measurements are taken at three different modes, temperature-scanned, pulse-rate-scanned, and time-scanned DLPTS. It is demonstrated that each mode provides unique information about the defect configuration, and the combination of the different modes offers a powerful tool for DLPTS studies of physical optoelectronic processes in SI-GaAs. The nonexponentiality/broadening of experimental data is extensively studied using the two prevalent broadening theories: the stretched exponential and the Gaussian distribution of activation energies. A hierarchical carrier emission model has been proposed for the stretched exponential behavior. Simulations indicate that the two broadening theories exhibit roughly similar broadening effects and good fits to the experimental data. The origin of this similarity indicates an ergodic equivalence of random energy distribution and the constrained hierarchical emission process. © *2009 American Institute of Physics*. [DOI: 10.1063/1.3131673]

I. INTRODUCTION

Deep level transient spectroscopy (DLTS), first introduced by Lang,[1] is a powerful tool for detection and characterization of deep-level generating defects in semiconductors. Several variations in the original capacitance transient method have been developed to make the measurement technique appropriate for specific material types and device structures. The principle of all these techniques is based on the rate-window resonance effect of temperature-dependent rates of defect state capture and emission processes. The systems under study have often been assumed to have a sharp, well-defined energy level, represented by a Dirac delta function, which leads to a single exponential decay in the ideal DLTS transient. This assumption, however, is not true for real semiconductor systems. In recent years, considerable amounts of work have been reported on the nonexponential behavior of DLTS transients.[2–5] The nonexponentiality is also observed in the temperature scans as a broadened spectrum.[6,7] Three models have been mainly proposed for the fitting of nonexponential data. These are the multiexponential model,[2,3] the William–Watts model,[4,5] and the distribution of defect parameters.[6,7] Although all these models have been successfully used for the fitting of experimental data, they are based on different physical assumptions and are usually studied independently without comparative evaluation. Since defect parameter identification and extraction depends on the type of measurement and model used to identify the defect, a study involving several complementary methods such as the one presented in this paper is important for enhancing the reliability of defect identification for the understanding of the physical phenomena in their own right as well as for the potential industrial applications of the new deep level photothermal spectroscopy (DLPTS) to SI-GaAs wafer characterization and optoelectronic quality control.

In earlier papers, we introduced an all optical DLPTS,[8,9] which utilizes a subbandgap laser to monitor the concentration of free carriers and the density of occupied states resulting from photoexcitation by a modulated coincident superbandgap laser beam. The technique was applied to semi-insulating (SI)-GaAs and a well-defined peak, associated with the EL3 level was observed in the above room temperature photothermal spectrum. The spectrum was then fitted by both simplified[8] and more comprehensive[9] theories. Although the comprehensive theory induced some broadening due to the consideration of carrier capturing processes, the experimental spectrum was still broader than the theoretical fits. In this paper, the DLPTS measurement is extended to low temperatures and experiments are performed in temperature, pulse-rate, and time domain. Theoretical models are presented for various modes of the DLPTS measurement, thus yielding a uniquely comprehensive study on the effects and possible physical origins of spectrum broadening theories.

II. OVERVIEW OF PHOTOTHERMAL SPECTRUM BROADENING THEORIES

The broadening of DLTS spectra is a common feature observed on various types of samples including semiconductor alloys,[6,10] plastically deformed silicon single crystals,[11,12] compound semiconductors,[7,13] and thin film layers.[14,15] A possible origin of this broadening is the distribution of defect parameters, such as activation energy and capture cross section. Mainly two models have been proposed for this distribution:[6,7] (i) the presence of compositional fluctuations due to the random distribution of specific atoms and (ii) the

a)Electronic mail: mandelis@mie.utoronto.ca.

fluctuating random Coulomb potential of the ionized shallow impurities. Due to the random nature of these phenomena, the distribution function is usually assumed to be Gaussian based on the central-limit theory.[6,7] Considerable amount of work has been done on DLTS systems with a Gaussian distributed activation energy and it has been suggested that defect parameters obtained from the conventional Arrhenius plots are also valid for weakly disordered systems.[6]

Other distribution functions have also been proposed in efforts to understand the actual physical origins of the energy spread. Teate and Halder[16] suggested a double exponential distribution in order to reflect disorder-induced band-tailing effects in shallow impurities. However, other studies suggested that this effect could better be interpreted as a correction factor on Gaussian distributions.[17] Batovski and Hardalov[18] pointed out that the distribution function could be more complicated and asymmetric in considering the spin degeneracy and lattice relaxation during the carrier capture and emission processes. They suggested an inverse theory to transform the thermal spectrum directly into a defect energy distribution spectrum. However, the transformation theory is ill-posed in nature and is not applicable for spectra with multiple levels. For these reasons, although the Gaussian distribution is based on an ideal configuration and its physical underpinnings are unclear, it is still the most widely used distribution function on broadening studies.

In the time domain, broadening is presented as a nonexponential transient. A convenient way of characterizing nonexponentiality is to write it in the form of a stretched exponential

$$I(t) \sim \exp[-(e_n t)^{\beta}]; \beta \leq 1, \tag{1}$$

where β is the stretching factor, $I(t)$ is the signal representing the transient, and e_n is the thermal emission rate of trapped carriers. For transients to yield a broadened spectrum, β should be less than one. This form of transient, also known as William–Watts decay,[19] has been invoked in many physical systems including dielectric materials,[20] polymers,[21] as well as semiconductors.[5,22,23]

Giri and Mohapatra[5] studied the nonexponentiality in SI-GaAs using an isothermal time-analyzed spectroscopy technique and found β to be smaller at lower temperatures. However, due to the limited number of sampling temperatures, they did not derive a direct relation between β and temperature. Yonekura *et al.*[22] studied the stretched exponential in the Laplace domain in an attempt to find its correlation with Gaussian distributions. Their study is based on the fact that the inverse Laplace transform of a stretched exponential function is the stable distribution $p(e_n, \beta, -\beta)$,[24] where

$$p(e_n, \beta, -\beta) = \frac{1}{\pi} \sum_{n=1}^{\infty} \frac{(-1)^n \Gamma(1+n\beta)}{n!\, e_n^{\beta n+1}} \sin\left[\frac{1}{2}\pi n(-2\beta)\right]. \tag{2}$$

For small β, the stable distribution can be approximated by a log-normal distribution. By comparing that distribution with the inverse Laplace transform of a Gaussian distribution in the activation energy, they found $\beta = kT/\delta E$, where δE is the standard deviation of the activation energy with a Gaussian distribution. However, this result is based on the assumption that β is very small ($\beta < 0.1$), while most studies reported $0.4 < \beta < 0.9$.[5,23]

Several physical models have been suggested to explain the stretched exponential behavior. Kim and Epstein[25] studied the depth dependence of a photogenerated defect population and expressed the final population as an integral over the optical penetration depth. They numerically solved the problem and proved that the simulated transient can be approximated by a stretched exponential. This model, however, cannot explain the temperature dependence of β.

Benatar *et al.*[23] proposed a parallel relaxation theory for the nonexponential behavior. In that theory, they also suggested a distribution of activation energies due to the local fluctuation around the defect site. Carriers with different activation energies were assumed to eject independently and the overall time constant was expressed as an integral over all emission rates with the distribution function as a weighting factor. The stretched exponential decay could be obtained by a suitable choice of the distribution/weighting function. This theory, however, neglects possible changes in activation energies during the emission/capture process (a constrained activation process). This activation energy variation, known as the Frank–Condon shift, is a result of changes in defect bonding energies caused by trap occupancy variation.[26] The energy shifts, which are usually small, could be significant for systems with highly fluctuating random potential energies[26] or large lattice relaxation.[27]

Contrary to parallel relaxation, Palmer *et al.*[28] proposed a hierarchical relaxation theory, which represents the hierarchy of constraints in systems. In this theory, degrees of freedom (DOFs) relax in series rather than in parallel; the slower DOFs are constrained by fast DOFs and are only activated when faster DOFs evolve in the right way. The dynamic model was evaluated with the saddle-point method and a stretched exponential relaxation was obtained with

$$\beta = 1/(1+\tilde{\mu}_0), \tag{3}$$

where $\tilde{\mu}_0$ is a spin number defined in the model. Palmer *et al.*[28] also pointed out that the constrained system had a maximum time scale $\tau_{\max}$ and the stretched exponential is only observable at $t < \tau_{\max}$. As time increases, the system will become more ergodic and will end up with a pure exponential decay relaxation when $t \gg \tau_{\max}$.

Despite the differences in physical origins, both Gaussian distribution theory and stretched exponential theory have been widely used in defect characterizations. Due to its direct relation to activation energies, the Gaussian distribution theory is mainly used on studying defect energy broadening. This energy distribution can be used to identify physical properties of the material, such as the concentration of metals in semiconductor alloys or the degree of disorder in a system.[6,10] On the other hand, β broadening is mainly used in time domain analyses. Due to its simple expression, it can be easily integrated into existing theories and studied analytically. For example, in time analyzed transient spectroscopy measurements,[5] the relation between the spectrum peak time and the thermal emission rate can be easily derived as in conventional temperature-scanned DLTS.[1,5] These calcula-

tions are usually more complicated or totally impossible in the Gaussian distribution theory. In terms of numerical simulations, our own results also indicate calculations with the Gaussian distribution theory take much longer than those with the stretched exponential theory.

Due to the temperature dependence of β, applications of the stretched exponential theory are usually limited to isothermal conditions.[5] As already mentioned, so far no physical $\beta(T)$ expression has been derived for semiconductor systems. In this paper, we propose such an expression for the temperature dependent β based on hierarchical dynamics and relevant to trapped carrier emission and/or capture processes in SI-GaAs. Its relation to a Gaussian distribution is verified using a wide range of DLPTS temperatures, frequencies, and transients accompanied by comparisons of experimental data to the theory.

III. PHYSICAL ORIGINS OF THE STRETCHED EXPONENTIAL IN SEMICONDUCTOR TRAP STATES

The thermal emission rate of carriers from a trap state at equilibrium can be written as a function of activation energy and temperature,[29]

$$e_n(T) = \phi(T)\exp\left(-\frac{E}{k_BT}\right), \tag{4}$$

where $\phi(T)=\gamma_n\sigma_nT^2$. γ_n is a material constant and σ_n is the capture cross section.

If the activation energy E changes during the emission/capture process due to electron-to-electron interactions, it is reasonable to assume E depends on the density of occupied states with a time-dependent energy.

$$E(t) = E_0 \pm \Delta E[n_T(t)]. \tag{5}$$

Here the $\pm$ sign means the activation energy may either increase or decrease. Even though the equilibrium condition itself becomes the asymptotic limit of a time-dependent carrier emission process, as long as $t \gg \tau_e$, where τ_e is the time to achieve equilibrium following an energetic adjustment of a trap energy state, a quasiequilibrium formalism would yield Eq. (4) with $e_n=e_n(T,t)$ and $E=E(t)$.

By further writing $\Delta E[n_T(t)]=\Delta E_0 f[n_T(t)]$, where f is a function to be determined, we obtain

$$e_n[T,n_T(t)] = \phi(T)\exp\left(-\frac{E_0}{k_BT}\right)\exp\left(-\frac{\pm\Delta E_0 f[n_T(t)]}{k_BT}\right)$$
$$= e_{n0}(T)\exp\left(-\frac{\pm\Delta E_0 f[n_T(t)]}{k_BT}\right). \tag{6}$$

Here $e_{n0}(T)=\phi(T)\exp(-E_0/k_BT)$ is the "ideal" thermal emission rate with a fixed activation energy E_0.

On the other hand, in order to obtain a stretched exponential decay, we require

$$e_n[T,n_T(t)]t = [e_{n0}(T)t]^\beta. \tag{7}$$

By rearranging the terms on both sides we have

$$e_n[T,n_T(t)] = e_{n0}(T)[e_{n0}(T)t]^{\beta-1}. \tag{8}$$

Since $n_T(t)=n_{T0}\exp\{-[e_{n0}(T)t]^\beta\}$, Eq. (8) can be written as

$$e_n[T,n_T(t)] = e_{n0}(T)\left(\ln\frac{n_{T0}}{n_T(t)}\right)^{\beta-1/\beta}. \tag{9}$$

By comparing Eq. (9) with Eq. (6), we deduce an expression for β,

$$\beta = \frac{\ln\left(\ln\frac{n_{T0}}{n_T(t)}\right)}{\ln\left(\ln\frac{n_{T0}}{n_T(t)}\right) + \frac{\pm\Delta E_0 f[n_T(t)]}{k_BT}}. \tag{10}$$

In order for β to be time-independent, the simplest functional form is obtained if we assume $f[n_T(t)]=\ln\{\ln[n_{T0}/n_T(t)]\}$, whence it follows that $\beta(T)=1/[1+(\pm\Delta E_0/k_BT)]$. Finally, for a broadened spectrum, β should be smaller than one. Therefore, it is shown that

$$\beta(T) = \frac{1}{\left(1+\frac{\Delta E_0}{k_BT}\right)}. \tag{11}$$

This β, which is of a similar form as Eq. (3) derived from a more general hierarchical model of constrained relaxation in strongly interacting dynamic ensembles,[28] also decreases as the temperature decreases in agreement with previous observations.[5] It should be noticed that ΔE_0 here reflects the variation in activation energy during the thermal emission/capture process and may not be equal to the standard deviation δE in the Gaussian distribution. In turn, $\Delta E_0/k_BT$ represents the number of electronic DOFs (measured in units of the carrier thermal quantum k_BT) available to each trapped carrier during the activation process of the trap. The equivalent quantity in other hierarchical quantum systems, like strongly interacting glassy materials,[30,31] is the number of spins at a given energy level. The nature of $E(t)$ as emission/capture processes under way change the activation energy for the remaining emission/capture events is consistent with the more general hierarchical origins of stretched exponentials in kinetic systems.[28] Based on these considerations, ΔE_0 depends on the local environment of interacting defect states under study and should have a correlation with energy distribution functions. The development of the DLPTS theory in the next section demonstrates that for equivalent energy-level broadening effects between stretched exponential, ΔE, and Gaussian, δE, distributions, $\Delta E_0 \approx \delta E/1.5$, and helps elucidate the physical implications of this equality. In what follows, we will refer to the hierarchically constrained dynamic β expression in Eq. (11) as β_2 and to the expression proposed by Giri and Mohapatra[5] as β_1.

IV. DLPTS SIGNAL GENERATION THEORY INCLUDING BROADENING EFFECTS

A detailed description of the DLPTS signal generation theory is given in an earlier paper.[9] Here, we will cover the basic elements and will integrate broadening into the theory. The DLPTS technique utilizes a sub-bandgap light to monitor the thermal recovery of defect states following a super-bandgap laser pulse. Two absorption mechanisms are considered here: free carrier absorption and defect absorption. Free carrier absorption is caused by injection of free carriers to

higher conduction band minima states and defect absorption is the result of excitation of trapped carriers (electrons) to the conduction band. Since the power of probe light used in DLPTS experiments is very low (<1 mW), it may be assumed that the absorption does not affect the overall occupancy of trap states. The probe light undergoes multiple internal reflections and scattering owing to the relative transparency of GaAs at the probe wavelength (1.5 μm) and the final signal in back-scattered DLPTS can be expressed as

$$I(t) \approx I_0 \frac{(1-R)^2 S(1-2\alpha_1 d_1)(1-2\alpha_2 d_2)}{1-RS} \approx K[1-2\alpha_1(t)d_1]; d_2 = d - d_1, \tag{12}$$

where $\alpha_1(t) = \sigma_{fca} n(t) + \sigma_{dla} n_T(t)$ is the absorption coefficient of sub-bandgap light, σ_{fca} and σ_{dla} are free carrier and defect optical capture cross sections, respectively, d_1 is the penetration depth of the super-bandgap light, d is the sample thickness, R is the reflection coefficient, and S is the scattering coefficient.

Carrier capture and emission processes can be represented by Shockley–Read–Hall rate equations.[29]

$$\frac{dn(t)}{dt} = G(t)_n^{\mathrm{op}} + \sum_{j=1}^{m} \{e_{nj} n_j(t) - C_{nj} n(t)[N_j - n_{Tj}(t)]\} - \frac{n(t)}{\tau_n}, \tag{13}$$

$$\frac{dn_{Tj}(t)}{dt} = -e_{nj} n_{Tj}(t) + C_{nj} n(t)[N_j - n_{Tj}(t)], \tag{14}$$

where $G(t)_n^{\mathrm{op}}$ is the optical generation rate, τ_n is the free carrier recombination lifetime, and for a defect level j, C_{nj} is the capture coefficient. N_j is the defect or trap concentration. By neglecting the retrapping of carriers and considering the fact that in SI-GaAs the recombination lifetime τ_n is much shorter than the inverse of the carrier emission and capture rates, the rate equations for optical excitation by a laser pulse simplify considerably and have approximate solutions:

For $t \le t_p$ (t_p is the laser pulse width),

$$n(t) = G^{\mathrm{op}} \tau_n (1 - e^{-t/\tau_n}), \tag{15}$$

$$n_T(t) \equiv \sum_{j=0}^{m} n_{Tj}(t,T) = \sum_{i=0}^{m} \frac{N_{Tj}}{1 + (e_{nj}/G^{\mathrm{op}} \tau_n C_{nj})} [1 - e^{-(G^{\mathrm{op}} \tau C_{nj} + e_{nj})t}]. \tag{16}$$

For $t > t_p$,

$$n(t) = \sum_{j=1}^{m} \frac{e_{nj}(E_j)}{\tau^{-1} - e_{nj}(E_j)} n_{Tj}(t_p)[e^{-(t-t_p)e_{nj}(E_j)} - e^{-(t-t_p)/\tau}] + n(t_p) e^{-(t-t_p)/\tau_n}, \tag{17}$$

$$n_{Tj}(t) = n_{Tj}(t_p) \exp[-e_{nj}(t - t_P)]. \tag{18}$$

The exponential decay in Eq. (18) represents the recovery of defect states after the optical pulse and that forms the basis for DLPTS measurements. Based on the broadening theories discussed above, assuming that each defect level has a Gaussian distribution in activation energy, Eqs. (17) and (18) can be generalized as

$$\begin{aligned} n(t) &= \sum_{j=1}^{m} \int_0^{E_g} n_{Tj}(t_p) \frac{e_{nj}(E_j)}{\tau^{-1} - e_{nj}(E_j)} [e^{-(t-t_p)e_{nj}(E_j)} - e^{-(t-t_p)/\tau}] \\ &\quad \times dE_j + n(t_p) e^{-(t-t_p)/\tau_n} \\ &= \sum_{j=1}^{m} \int_0^{E_g} \frac{N_{Tj} g(E_j)(1 - e^{-(nC_{nj} + e_{nj})t_p})}{1 + e_{nj}(E_j)/(nC_{nj})} \frac{e_{nj}(E_j)}{\tau^{-1} - e_{nj}(E_j)} \\ &\quad \times [e^{-(t-t_p)e_{nj}(E_j)} - e^{-(t-t_p)/\tau_n}] dE_j + n(t_p) e^{-(t-t_p)/\tau_n}, \end{aligned} \tag{19}$$

$$n_{Tj}(t) = \int_0^{E_g} n_{Tj}(t_p) \mathrm{e}^{-e_{nj}(E_{nj})(t-t_p)} dE_j, \tag{20}$$

where E_g is the bandgap energy and $g(E_j, \delta E_j)$ is the Gaussian distribution function with average energy E_j and standard deviation δE_j.

In the stretched exponential case, a straightforward generalization of Eqs. (17) and (18) yields

$$n(t) = \sum_{j=1}^{m} \frac{e_{nj}}{\tau^{-1} - e_{nj}} n_{Tj}(t_p) \{e^{-[(t-t_p)e_{nj}]^{\beta_j}} - e^{-(t-t_p)/\tau_n}\} + n(t_p) e^{-(t-t_p)/\tau_n}, \tag{21}$$

$$n_{Tj}(t) = n_{Tj}(t_p) \exp\{-[e_{nj}(t - t_P)]^{\beta_j}\}. \tag{22}$$

To demonstrate the photothermal spectrum broadening effect induced by β and the energy broadening, Fig. 1 shows simulations of various broadening theories at 4 kHz pulse repetition frequency. In DLPTS the repetition frequency of the photocarrier excitation optical pulse acts like a rate window, which becomes resonant with optoelectronic kinetic processes in a semiconductor under investigation when the repetition rate is tuned to emission or capture rates of photocarriers. The attainment of such resonances results in trap specific temperature peaks on a photothermal spectrum such as that shown in Fig. 1. Since β is temperature dependent, three activation energies were chosen in order to cover the full temperature range. The simulation is based on semi-insulating GaAs with a single defect level. All three defect levels in Fig. 1 are assumed to have the same parameters except for the activation energy. Parameters used for simulation are listed in Table I.

Figures 1(a) and 1(b) demonstrate broadening effects at low temperatures. In those temperature ranges, all three broadening theories yield similar results, both spectral lineshapes and linewidths. In Fig. 1(a), the Gaussian distribution gives a gradual decay tail on the high temperature side, which is not seen with β type broadening. This asymmetric distribution is due to the nonlinear dependence of e_n on E as shown in Eq. (4). When the temperature increases, that effect becomes less significant. The linewidth of the β_1 spectrum decreases as the peak shifts to high temperatures with increasing activation energy, and in Fig. 1(c), it becomes even narrower than the nonbroadened spectrum. This is consistent with our discussion above, since β_1 broadening is derived based on the assumption that it is a small parameter (<1). As

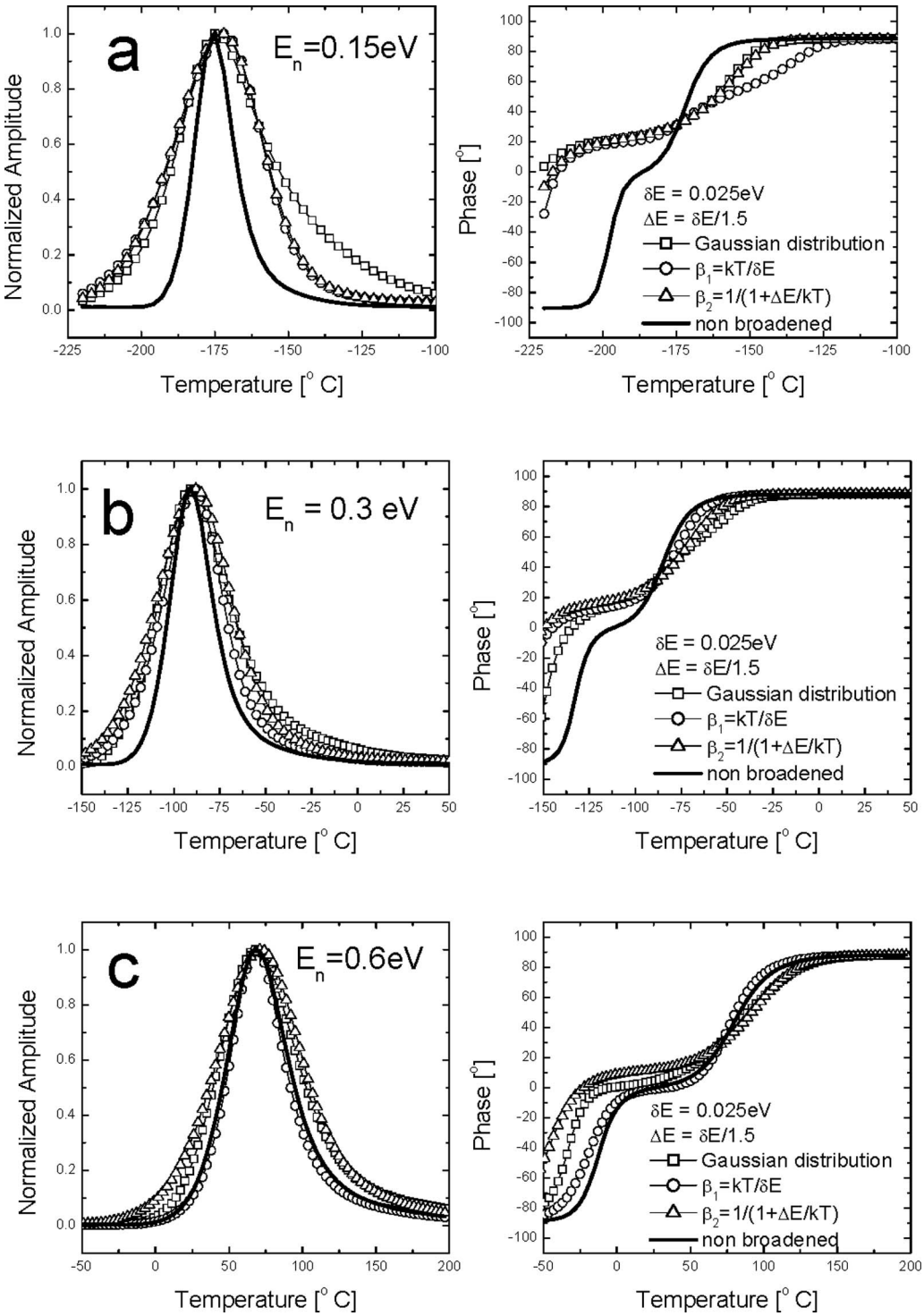

FIG. 1. Theoretical simulations of photothermal spectrum broadening under three broadening mechanisms. Insets: δE is the spread (standard deviation) of trap energy Gaussian distribution; ΔE is the spread of the β_2 broadening.

the temperature increases, β_1 will eventually become larger than one and no longer give a broadened spectrum. Compared to β_1, the theoretical spectrum with β_2 broadening is more comparable with the Gaussian distribution at all temperature ranges. Discrepancies are mainly shown at low temperatures, where the Gaussian spectrum tends to be broader

TABLE I. Fitting parameters for simulations shown in Fig. 1 (Ref. 9).

	σ_{fca} (cm^2)	g_{op} (cm^{-3} s^{-1})	τ_n (s)	γ_n (cm^{-2} s^{-1} K^{-2})	σ_n (cm^2)	σ_{dla} (cm^2)	N_T (cm^{-3})
SI-GaAs	3×10^{-18}	2×10^{23}	1×10^{-8}	2.67×10^{20}	2.7×10^{-13}	1×10^{-16}	0.5×10^{15}

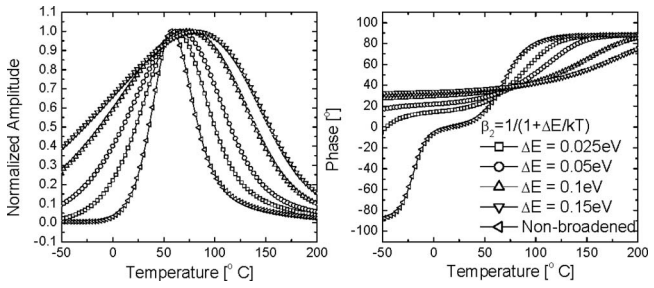

FIG. 2. Simulated DLPTS β_2 broadening at various ΔE.

than the β_2 spectrum. As a result, for equivalent broadenings at low temperatures, the ratio $\delta E/\Delta E$ should be smaller than 1.5. As will be seen in later sections, this observation is consistent with theoretical fits of photothermal spectra.

A slight shift to higher temperatures in peak position for the β_2 amplitude spectrum is also apparent. This is due to the asymmetric distribution of β_2 around the peak in the temperature scan. For the spectrum with Gaussian distribution, the peak position remains fixed. This β_2-induced displacement could affect trap identification, since, on an Arrhenius plot, a shift to higher temperature means an overestimation of activation energy. It also means that, without due consideration of broadening effects, activation energies measured heretofore from Arrhenius plots may be inaccurate. Figure 2 shows changes in amplitude peak position under β_2 broadening for various ΔE. Large shifts are only observed at $\Delta E \geq 0.1$ eV. Experimentally it was found that most of the identified energy levels have $\Delta E < 0.05$ eV, which implies the activation energy derived from the Arrhenius plot is accurate for weakly stretched photothermal spectra. However, for large spreads in trap energies, a correction factor needs to be added to the Arrhenius plot based on broadening in order to obtain accurate mean activation energies.

V. EXPERIMENTAL SYSTEM FOR DLPTS

The schematic of the DLPTS experiment is shown in Fig. 3. The sample is placed on a Linkam LTS350 cryogenic stage, which allows maintaining constant temperature in the −196 to +350 °C range, or can provide temperature ramping. The excitation source is a periodic time-gated superbandgap laser pulse ($\lambda = 830$ nm) emitting 20 mW (peak power) with a beam diameter of about 0.1 mm. The pulse parameters are controlled by a pulse generator, with the pulse width fixed at 1% of the repetition period. Due to the high absorption coefficient of the superbandgap beam ($\alpha \sim 10^4$ cm^{-1}), the pump laser penetrates only a few micrometers into the sample. The probe beam is from a coincident sub-bandgap unmodulated laser ($\lambda = 1550$ nm) emitting 1 mW with approximately 0.15 mm diameter spot size. Samples used in this work are one-side-polished vertical gradient freeze grown SI-GaAs wafers with a resistivity of $7.2–7.7 \times 10^7$ Ω cm, etch pit density <4000 cm^{-2}, and EL2 concentration around 10^{16} cm^{-3}, as provided by the vendor. The probe laser penetrates the entire thickness of the SI-GaAs wafer, it is partly absorbed and scattered by the naturally rough (matte) back surface of the sample. The scattered light is collected by two collimating off-axis paraboloidal mirrors and focused onto an InGaAs photodetector with a 1550 nm narrowband filter. For temperature- and pulse-rate-scanned DLPTS (switch a, Fig. 3), the signal is fed into an AMETEK 5210 lock-in amplifier, which functions as a rate window, while for time-scanned DLPTS (switch b, Fig. 3), the raw signal is collected through a National Instruments PCI-6281 data acquisition card installed in the computer. The results are displayed simultaneously in the computer as a function of temperature, pulse-rate, and time, respectively.

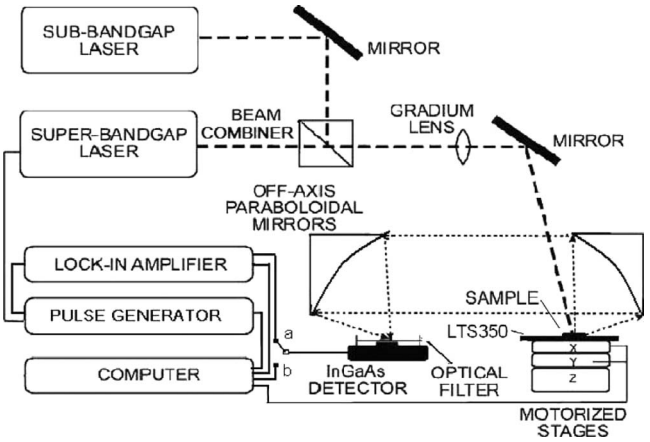

FIG. 3. Schematic for DLPTS: (a) temperature and frequency scanned modality and (b) time-scanned modality.

VI. EXPERIMENTAL RESULTS AND DISCUSSION

A. Photothermal temperature spectra

Figure 4(a) shows the DLPTS temperature-scanned spectra at various pulse repetition frequencies. For a clear view of the data, spectra contains only the cooling cycle. In the following simulations, both the cooling and heating cycles of experimental data are shown. There are two major peaks (see arrows) in the amplitude photothermal spectrum. The peak height decreases as the frequency increases. This is caused by the decrease in pulse width, which reduces the number of injected carriers. However, the peak resolution increases with increasing frequency. The phase spectrum shows inverted peaks (see arrows) in both low and high temperature regions. The peaks also shift to higher temperatures as the frequency increases. However, unlike the DLPTS amplitude, the peak-to-trough phase shift does not change much as the frequency increases. This behavior is consistent with the carrier density-wave phase independence from the carrier flux (the latter is proportional to the laser intensity).[32]

It should also be noticed that there is a huge increase in the amplitude spectrum at temperatures lower than −160 °C. The origin of the increase is not the onset of another defect peak. Considering the temperature dependence of bandgap energy in GaAs.[29]

$$E_g(T) = 1.519 - 5.405 \times 10^{-4} T^2/(T + 204), \tag{23}$$

$T = -160$ °C corresponds precisely to $E_g = hc/\lambda$, the photon energy at $\lambda = 830$ nm (emission wavelength of the laser). Below this temperature, the bandgap energy is larger than the photon excitation energy, which converts SI-GaAs to an almost transparent medium. For $T \leq -160$ °C the DLPTS sig-

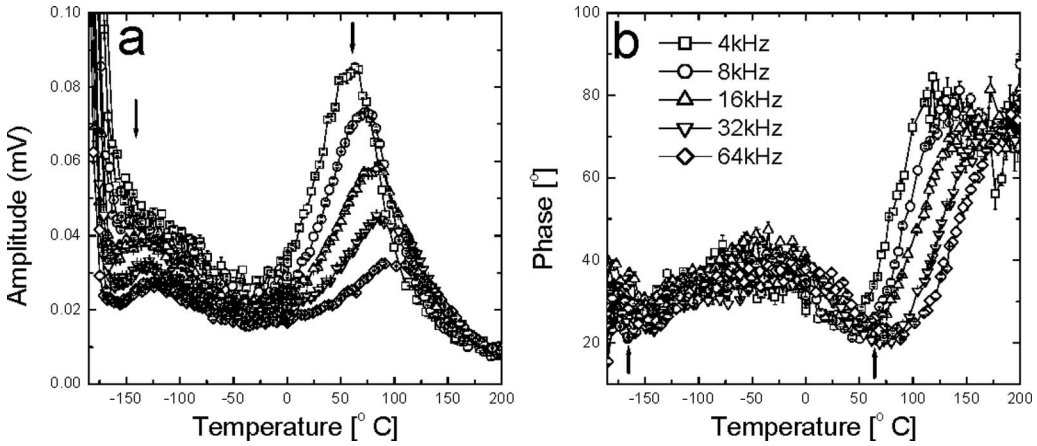

FIG. 4. Temperature-scanned DLPTS spectra of SI-GaAs at various pulse (1% duty cycle) repetition frequencies.

nal generation theory must be modified. The absorption coefficient under this condition can be expressed by Urbach's rule, which represents an exponential decay as a function of bandgap energy as shown in Eq. (24).[33]

$$\alpha = \alpha_0 \exp\left[\frac{\varepsilon(E_{\text{op}} - E_g)}{k_B T}\right]. \tag{24}$$

Here E_{op} is the energy of photon, ε and α_0 are material constants. In terms of optical penetration depth $(d=1/\alpha)$, which amounts to an exponential increase as the temperature decreases. Based on that, there are two possible explanations for the sharp increase at low temperatures: (a) the 830 nm laser penetrates deeper into the sample, thus enhancing the DLPTS signal modulation depth by considerably increasing the absorptance $\alpha_1(t)d_1$, as expressed in Eq. (12); or (b) the 830 nm laser excites carriers directly to shallow defect traps instead of the conduction band, which enables a higher trap population modulation. Since the low temperature peak is more likely to be an exponential increase as represented by Urbach's rule, we believe the former mechanism is more appropriate for this phenomenon. Using Eqs. (12)–(24), Fig. 5 shows the simulated DLPTS amplitude spectrum at low temperature. As it can be seen, the Urbach theory nicely predicts the low temperature amplitude increase. In order to show details of the high temperature data, our following discussion will be focused on spectra above −160 °C.

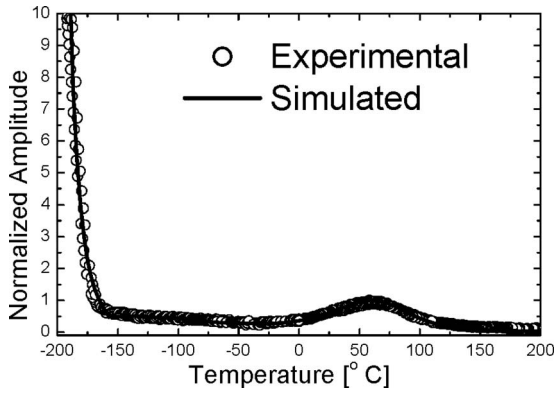

FIG. 5. Theoretical and experimental DLPTS spectra showing Urbach effect at low temperature.

The thermal emission rate at each peak temperature can be calculated by $e_n(T_{\text{peak}})=2.869f$,[8] where $f=1/T_0$ is the pulse repetition frequency. Based on Eq. (4), the two defect peaks in Fig. 4(a) are identified from the Arrhenius plot shown in Fig. 6. Using the nonbroadened theory, Eqs. (15)–(18), the simulated DLPTS spectrum with two defect levels is shown in Fig. 7. The theoretical amplitude spectrum shows two peaks as expected, however, they are much sharper than the experimental peaks and the amplitude between the two is almost zero. Similarly, the theoretical phase spectrum shows little resemblance to the data. Considering that there are many more levels in SI-GaAs besides the two apparent peaks, it is expected that the experimental spectrum reflects the superposition of several defect states. Since the defect states in SI-GaAs have already been well identified by other techniques,[34,35] more levels were included into our simulation. In view of the fact that the defect optical cross sections (σ_{dla}) are not known in SI-GaAs, as a starting point they were assumed to be the same as the value shown in Table I. As can be seen from Eqs. (12), (16), and (18), this assumption only affects the trap concentration identification and can be easily corrected once σ_{dla} are determined through optical absorption measurements.

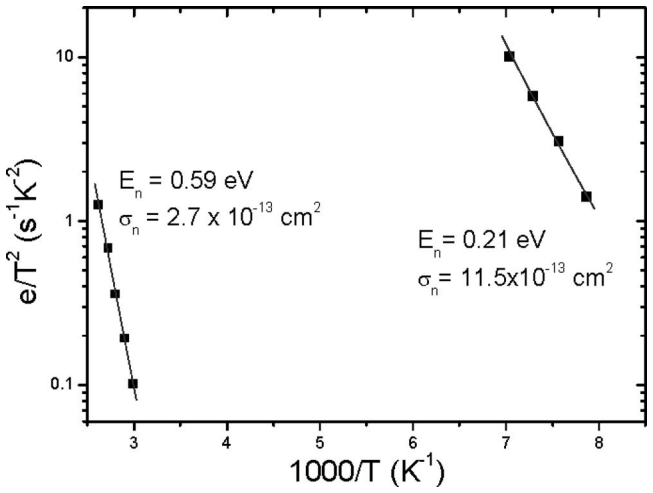

FIG. 6. Arrhenius plot of the two DLPTS amplitude peaks shown in Fig. 4.

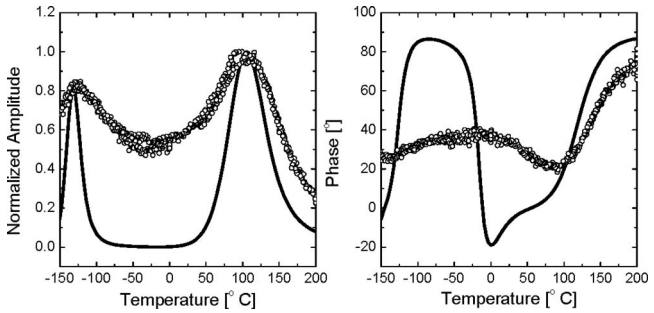

FIG. 7. Theoretical DLPTS spectrum with two levels at 64 kHz pulse repetition rate, superposed on the photothermal spectrum (including both cooling and heating cycles) of Fig. 4(a).

After adjusting the defect concentrations and capture cross sections for optimal (best) fits of the theory to the experimental photothermal spectrum, the DLPTS spectra shown in Fig. 8 were obtained. The fitting parameters are summarized in Table II and the defects are identified according to the literature.[34,35] It should be noticed that parameters for HL3 and EL2 levels are determined from the phase spectra only, which will be discussed in detail later. Compared with the two-level theory, the superposition of more defect levels[9] gives considerably improved fits to the experimental spectrum in both amplitude and phase. However, the theoretical spectrum shows several well-resolved peaks. Although more defect states could be introduced in order to yield a smooth spectrum, doing so results in nonexistent defects in SI-GaAs. Observations here are consistent with our earlier paper,[9] which indicated multiple levels cannot explain the DLPTS spectrum unless broadening mechanisms are considered.

Without introducing more levels, the fits can be significantly improved by use of the broadening theories introduced above. Since it was demonstrated in Sec. IV and Fig. 1 that β_1 type broadening has a limited temperature range, the following discussion will be based on Gaussian [Eqs. (19) and (20)] and β_2 [Eqs. (21) and (22)] types of broadening only. By independently adjusting δE for each level, Fig. 9(a) gives the best fit of the experimental spectra with Gaussian broadening and Tables II and III show the fitting parameters. Defect peaks are broadened and eventually disappear due to superposition with other peaks. The data were also fitted with stretched exponential β_2 broadening. In this fitting, the electrons or hole energy level parameters were kept the same as the Gaussian fitting and $\Delta E_n = \delta E_n / 1.5$ was set as the initial value. Since every defect level has its own characteristic peak temperature corresponding to a rate-window resonance at fixed frequency, each ΔE_n can be independently adjusted for best fitting. The results with β_2 broadening are shown in Fig. 9(b). Table III gives a summary of ΔE_n and δE_n associated with β_2 and Gaussian broadening, respectively. The two theories give similar peak contribution results and both fit very well at all frequencies.

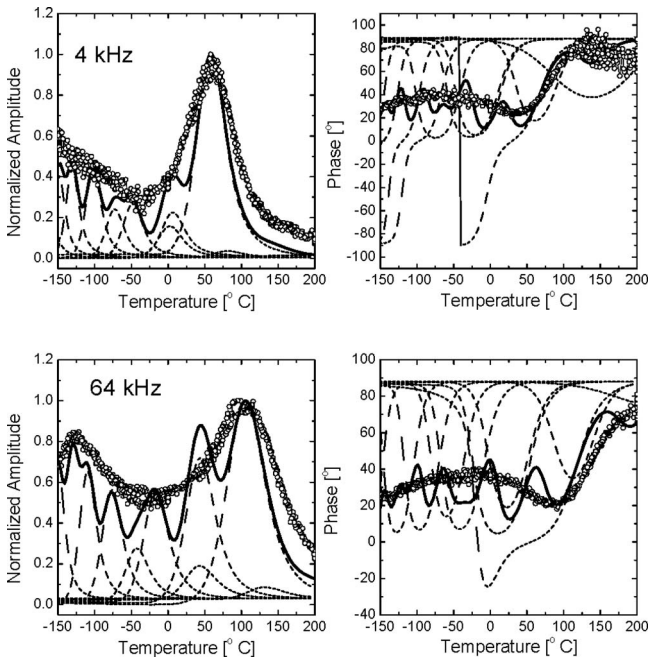

FIG. 8. Temperature scanned DLPTS at 4 and 64 kHz shown the superposition of eleven defect peaks. Defect states and their parameters are shown in Table II. The continuous line is the superposition spectrum.

TABLE II. Summary of defect states detected by DLPTS.

	E_n (eV)	σ_n (1×10^{-13} cm^2)	N_T [a] (1×10^{15} cm^{-3})
EL2	0.76	6.0	0.03
HL3	0.65	6.7	0.03
EL3	0.58	2.7	1.0
EL4	0.52	13.67	0.2
EL5	0.48	3.53	0.15
HB5	0.40	8.39	0.239
EL6	0.34	4.0	0.232
EB7	0.29	5.38	0.40
EL14	0.24	7.0	0.40
EL17	0.21	9.4	0.364
EL11	0.17	5.43	0.64

[a]The defect concentration needs to be corrected by the absorption cross section of the defect state.

The similarities between the two broadening configurations offer major physical insight. Ergodic systems are equilibrium statistical ensembles in which time statistics is equivalent to statistics based on energetically random distributions in an appropriate phase space of microstates. The experimental proof of validity of an ergodic hypothesis in the case of trapped carriers in SI-GaAs and other semiconductors is tantamount to a statement that all accessible trap microstates are equally probable over a long period of time.[36] This period can be of the order of the time required to empty (emission) or fill (capture) the trap and it is much longer than the interaction time among the member electron or hole population of a trap or defect. The existence of this type of equivalence in the case of semiconductors and SI-GaAs in particular as revealed by temperature-scanned DLPTS, points to a photocarrier ensemble statistical ergodic relationship, and thus renders the Gaussian energy distribution a meaningful statistical mechanical quantity. The nature of the trapped carrier ergodicity needs to be investigated further.

In Table III, the ratio between δE and ΔE is 1.5 for most defect levels. Some discrepancies exist on shallow (small

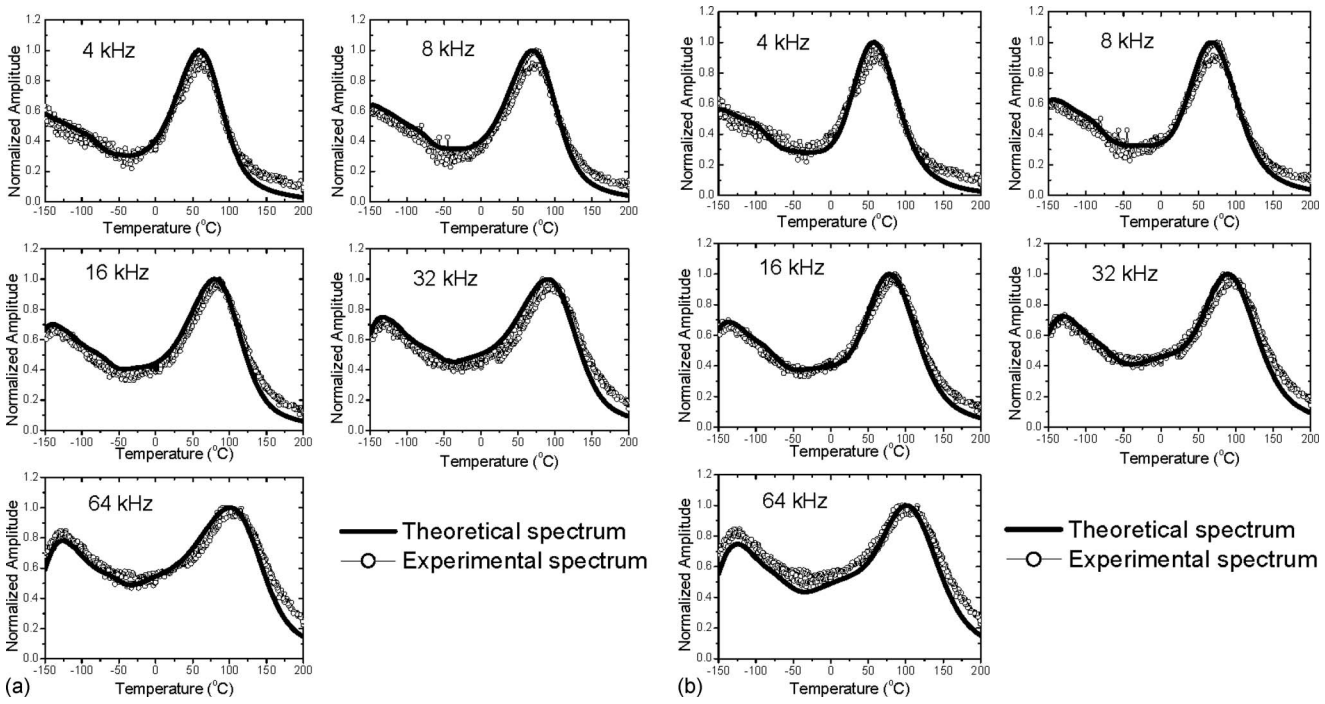

FIG. 9. Experimental (including both cooling and heating cycles) and theoretical temperature-scanned DLPTS amplitude spectra at various pulse repetition frequencies. (a) Theory with Gaussian activation energy broadening. (b) Theory with stretched exponential β_2 broadening.

activation energy) defect levels, where the ratios are significantly smaller than 1.5. Considering semiconductor systems are usually less disordered at low temperatures than at high temperatures, observations here indicate that the statistical relation between δE and ΔE is influenced by the degree of disorder in the system and defines the temperature extent of ergodicity. The obvious ergodic inference of the relation $\delta E = \text{const.} \times \Delta E$ is that the extended electronic carrier microstate distributions within the trap levels for which the relation holds are equivalent to the hierarchical emission/capture kinetics of the carrier ensemble out of/into the energy distributed levels, respectively. An analogous phenomenon has been observed in the case of luminescence time decay in porous silicon as function of temperature and energetics of localized states.[37] The extended trap theory and its linkage to a stretched exponential Kohlrausch relaxation parameter has been established for carrier relaxation in semiconductor Cd_xSe_{1-x} nanocrystallites.[38] In all these cases the underlying cause of ergodicity is the effect of soft potentials within the trap state, which allows the existence of different interaction spatial scales.[39] This phenomenon can only be quantified with noncontact multimodal techniques such as DLPTS, which allow testing of the ergodic hypothesis through temperature, pulse-rate, and time-scanned measurements involving trapped carrier ensembles in extended states and dynamic/kinetic statistical rates.

TABLE III. Summary of standard deviation δE (Gaussian broadening) and ΔE (stretched exponential) β_2 broadening.

	δE (eV)	ΔE (eV)	$\delta E/\Delta E$
EL2	0.06	0.04	1.5
HL3	0.03	0.020	1.5
EL3	0.035	0.021	1.67
EL4	0.075	0.05	1.5
EL5	0.083	0.055	1.5
HB5	0.068	0.055	1.24
EL6	0.057	0.038	1.5
EB7	0.032	0.027	1.19
EL14	0.029	0.027	1.07
EL17	0.027	0.025	1.08
EL11	0.024	0.025	0.96

Defect states identified in Table II are also consistent with independent measurements on the same SI-GaAs wafer.[40] Using the piezoelectric photothermal (PPT) technique,[41] Ikari and Fukuyama identified defects from HL3 to EL6. However, the defect state characteristic temperatures in the PPT spectrum are much lower than those in the DLPTS spectrum. Within the same temperature range, they did not observe defects shallower than EL6. This variation in the defect characteristic temperature reflects the different probing principles of the two techniques. As pointed by Look,[42] for techniques monitoring the defect occupancy $n_T(t)$, such as in capacitance DLTS,[1] resonance occurs at $e_n = 2.36f$, and for techniques monitoring the free carrier concentration $n(t)$, such as in photoinduced transient spectroscopy (PITS),[34] resonance occurs at $e_n = 6.35f$. For this reason, the defect peak temperatures in $n_T(t)$-probing techniques are always higher than those of $n(t)$-probing techniques. As will be seen in Sec. VI C, DLPTS monitors both $n_T(t)$ and $n(t)$, with $n_T(t)$ being the major contribution to the signal, therefore the defect resonance temperature is higher than other $n(t)$-probing techniques. This also reflects a practical advantage of DLPTS, as high temperature measurements are usually more accessible than low temperature measurements.

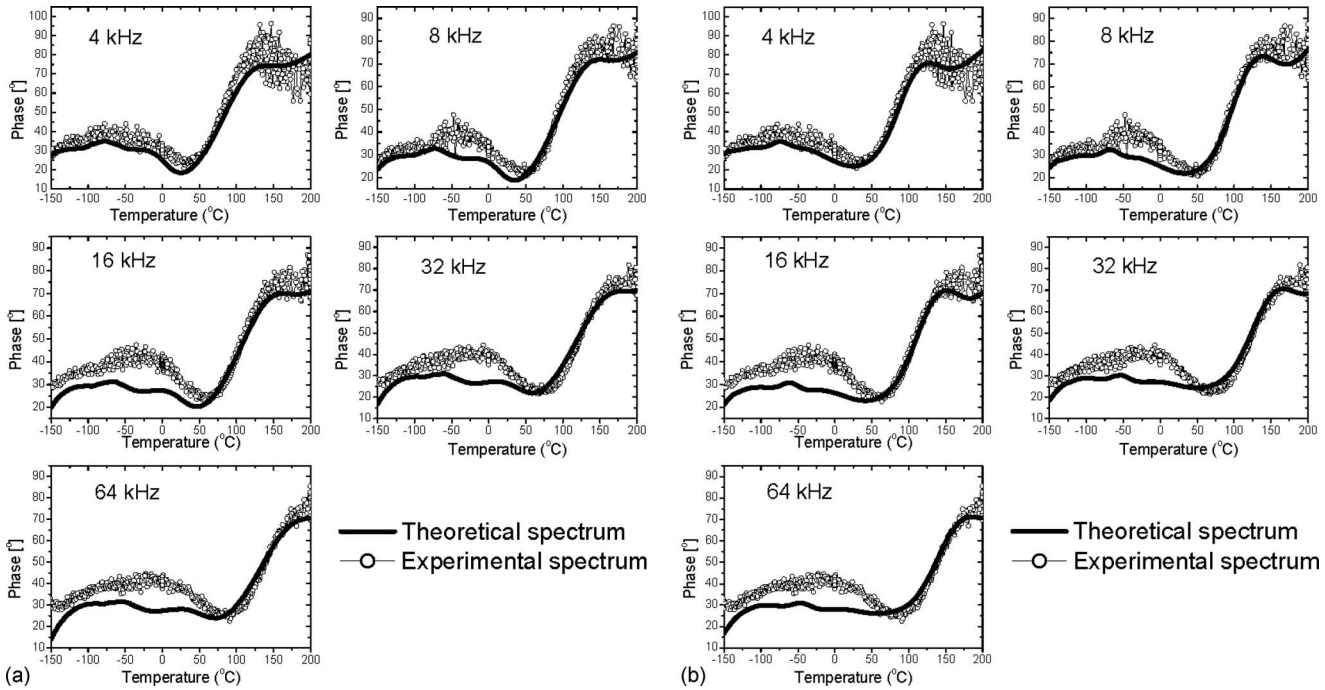

FIG. 10. Experimental (including both cooling and heating cycles) and theoretical temperature-scanned DLPTS phase spectra at various pulse repetition frequencies. (a) Theory with Gaussian activation energy broadening. (b) Theory with stretched exponential β_2 broadening.

Using the same fitting parameters in Tables II and III, Fig. 10 shows experimental and theoretical phase spectra. The latter spectra are neglected in most DLTS based techniques, mainly because the phase spectrum does not exhibit defect peaks like the amplitude spectrum. However, simulations in Fig. 8 demonstrate that each peak in the amplitude spectrum has a correlated reversed peak in the phase spectrum and the phase-peak temperature is always around 25 °C lower than the amplitude-peak temperature. This observation indicates that within same temperature ranges the phase spectrum is capable of identifying deeper levels (higher activation energy) than the amplitude spectrum. In Fig. 10, an unexpected decrease at the high temperature end can be seen in the 4 kHz phase spectrum. According to Fig. 8, this decrease is most likely due to the onset of another phase peak. Simulations on the broadened DLPTS theory indicate the decrease is due to the superposition of the HL3 and EL2 levels. The HL3 level controls the turning point of this decrease and the EL2 level determines the slope of the decrease. The EL2 concentration in Table II is much lower than the value provided by the vendor (10^{16} cm^{-3}). As mentioned earlier, defect concentrations in Table II need to be corrected by the actual value of the absorption cross section σ_{dla}. Since the σ_{dla} of EL2 level is much smaller than 10^{-16} cm^2 at the 1550 nm (0.8 eV) probe wavelength,[43] the EL2 concentration here is underestimated. According to the EL2 absorption spectrum in Ref. 43, the corrected EL2 concentration will be at least 3×10^{15} cm^{-3}, which is close to the magnitude provided by the vendor.

The fact that the 1.5 μm laser has low absorption on EL2 level is the main reason of choosing that wavelength. The EL2 level has been intensively studied during the past few years using optical absorption methods with 1 μm wavelength probe.[43] However, due to the high absorption from the EL2 level, other defect states cannot be identified from those absorption spectra. The 1.5 μm laser, which represents the onset wavelength of EL2 absorption,[43] limits the absorption from EL2 level and enables proper identification of other shallower defects. Also, since the EL2 level is known to be a source of photoexcited electrons,[41] using a laser with high EL2 absorption will induce significant interband carrier transportations, which will disturb the carrier distribution generated by the 830 nm laser and make theoretical analysis to be more complicated.

For both types of broadening, photothermal phase spectroscopic theory fits the data better at lower frequencies than at higher frequencies. Since a higher pulse repetition frequency at fixed laser power means lower optical excitation energy, observations here indicate the phase spectrum could be more sensitive to optical energy in the DLPTS technique. Similar results are observed in pulse-rate-scanned DLPTS, Sec. VI B, indicating a close relation between photothermal temperature-scanned phase spectrum and pulse-rate scans.

It should be noticed that the best-fit parameters to DLPTS spectra presented here are primarily based on the temperature-scanned spectrum, however data from other DLPTS modalities have been derived and used. The optical generation rate, $G^n_{\mathrm{op}}(t)$, used here is determined from the pulse-rate scans, and the relative contribution of $n(t)$ and $n_T(t)$ absorption is determined from the time-domain transients. As a result, Tables I–III reflect the final best fitting parameters and were also used in the pulse-rate and time-domain theoretical fits. A detailed discussion of these parameters is presented in the following sections.

B. Pulse-rate-scan spectra

In addition to the most commonly used temperature-scan modality, we also introduce two other modes of DLPTS

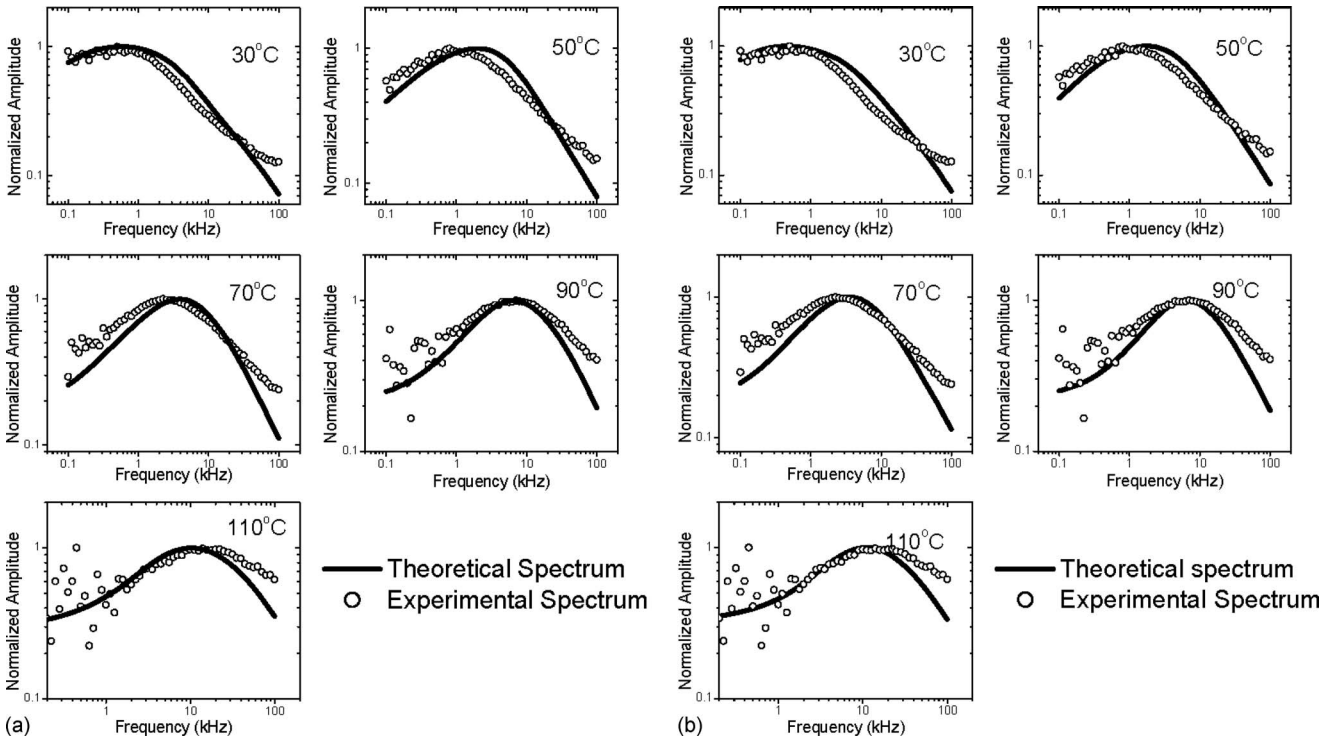

FIG. 11. Experimental and theoretical pulse-rate-scanned DLPTS spectra at various temperatures. (a) Theory with Gaussian activation energy broadening. (b) Theory with stretched exponential factor β_2 broadening.

theory and measurements, namely, pulse-rate and time-domain DLPTS. Pulse-rate-scanned DLPTS is the inverse of temperature-scanned DLPTS. In this case, the pulse repetition frequency is scanned at various temperatures while keeping the laser pulse duty cycle fixed at 1%. A detailed DLTS study of pulse-rate scans was reported by Henry *et al.*[44] They theoretically presented a three dimensional DLTS spectrum with the *x*-axis as temperature, *y*-axis as pulse-rate, and *z*-axis as signal amplitude. After comparing the pulse-rate and temperature ranges for specific defects, they found the pulse-rate scan requires a much wider range ($10^{-6}-10^{6}$ Hz) in order to cover the full defect-state spectrum of a *n*-type neutron irradiated silicon.

Similar observations were made in our DLPTS pulse-rate scan. The pulse-rate spectra in Fig. 11 exhibit a broad peak, which shifts to higher pulse rates as the temperature increases, instead of the two distinct peaks of the photothermal temperature spectra, Figs. 4 and 9. The theoretical fits indicate this peak corresponds to the EL3 level, which is also the above room temperature peak in the photothermal temperature spectrum. The low temperature peak (EL11 level) of Fig. 9, however, cannot be seen in this pulse-rate range. The theoretical consistency of the EL3 peak positions between temperature-scanned and pulse-rate-scanned DLPTS spectra enhances the trap energy state diagnostic capability of DLPTS over other single-scan methodologies. This self-consistency check can only be made by comparing the photothermal pulse-rate scan with the temperature spectrum. In the temperature spectra, the EL3 level resonance peak appears above room temperature in a pulse-rate range of several kilohertz, whereas at the same pulse rate, the EL11 level peak appears at around −140 °C. Therefore, in order to observe the EL11 peak in the pulse-rate scan, one should either decrease the sampling temperature to around −140 °C, or extend the pulse-rate range to GHz (the room-temperature emission rate of EL11 level), which is beyond the bandwidth limits of our lock-in amplifier (120 kHz), and very likely below the noise floor of the photothermal experiment.

Using Eqs. (19)–(22), theoretical pulse-rate-scanned spectra are also shown in Fig. 11. They were obtained at a fixed temperature from DLPTS signals using the 1% laser pulse duty cycle and scanning the pulse repetition rate $f = 1/T_0$. It can be seen that the two broadening theories give similar results in the pulse-rate scans in further agreement with the ergodic considerations of the trapped photocarrier ensemble. The theoretical pulse-rate scan predicts the peak position shift to higher pulse-rates with increasing temperature, as expected. Discrepancies, mainly in the high pulse-rate regime, are reflected as a narrower theoretical peak than the experimental one. Compared with the temperature-scanned results, these discrepancies could be related to the disagreements between theory and experiment at high pulse-rates in the temperature phase spectrum. Origins of these discrepancies are likely due to the approximations used in deriving the time domain theory. As mentioned in our earlier paper,[9] the total electronic thermal transport rate is a combination of the thermal emission and capture components. Although the capture components are usually small and can be neglected, their effects could become more significant at higher pulse rates. To overcome this, a harmonic frequency-domain analysis has been developed by Fourier transforming the rate Eqs. (19)–(22) into their frequency domain counterparts. In this case the coupled differential rate equations are converted into algebraic equations, which can be solved ana-

lytically without approximations. A detailed discussion of harmonic frequency-domain analysis and fitting to data will be presented elsewhere.

Although pulse-rate-scanned DLPTS has limited applications due to the requirement of wide detection bandwidth, it can be partially improved by using a wide bandwidth lock-in amplifier (current lock-in amplifier technologies provide detection up to 200 MHz). By judiciously choosing the temperature, pulse-rate-scanned DLPTS may be used for defect-specific analysis, since the influence of other defect states can be filtered out by gating the frequency (or pulse repetition rate) bandwidth. For the scans shown in Fig. 11, theoretical simulations indicate that changing the EL5-EL11 parameters has almost no effect on the best-fit process. Pulse-rate-scanned DLPTS also has several other advantages over the temperature-scanned modality. As mentioned earlier, unlike the temperature spectra, the peak position in the pulse-rate spectrum is sensitive to the optical generation rate, $G_{\mathrm{op}}^{n}(t)$, where a higher $G_{\mathrm{op}}^{n}(t)$ shifts the peak to higher frequencies. Although $G_{\mathrm{op}}^{n}(t)$ could in principle be calculated from the laser power, the actual amount of light entering the sample after reflection and scattering is hard to determine. Our fitting of the pulse-rate domain spectrum indicates $G_{\mathrm{op}}^{n}(t)$ takes on only half of the calculated value. This fact helps determine the actual optical power that couples into the sample and also turns pulse-rate DLPTS into a useful tool for power sensitive optoelectronic measurements. In addition, pulse-rate-scanned DLPTS measurements are performed under isothermal conditions, which are very useful for precision analysis of temperature-sensitive defect state kinetics.

C. Time-domain transients

The DLPTS time-domain transients were collected under conditions identical to the temperature-scanned and pulse-rate-scanned DLPTS by a National Instruments data card and were averaged by a LABVIEW program by over 100 000 times in order to obtain a high signal-to-noise ratio. The advantage of transient DLPTS is that it represents the raw signal as captured by the photodiode detector and provides a direct way of verifying the fitting parameters in Table II. Using Eqs. (19)–(22), Fig. 12 shows experimental and theoretical DLPTS transients at various temperatures. All transients consist of three parts, (a) a sharp decrease in the signal at the beginning of the pulse, followed by (b) a rapid recovery of the signal at the end of the pulse, and further followed by (c) a slower long-time recovery of the signal. The rapid decrease is caused by the generation of free carriers from the excitation pulse, which increases the infrared absorption coefficient and thus decreases the DLPTS signal in diffuse reflection from the back surface after a round trip across the bulk of the semiconductor. The fast increase is due to the recombination of free carriers and restoration of the near-infrared transparency of the semiconductor, while the slow recovery is a result of thermal emission of carriers from deep energy states in the bandgap.[9]

It can be seen that both broadening theories give excellent fits to transients at all temperatures thus further supporting the ergodicity of the thermal emission process from the active trap state(s). There are only small discrepancies at certain temperatures. However, the discrepancies are negligible compared to those observed in the temperature-scanned and pulse-rate-scanned spectra. This fact indicates that the transient DLPTS response has the lowest energy-state resolution and is not sufficient for the study of multiexponential or stretched exponential decays. This conclusion has far-reaching consequences, as transients obtained at fixed temperature are the commonest diagnostic modality in conventional electronic deep-level studies of semiconductors [for example digital PITS (Ref. 3)]. To overcome this lack of resolution, some researchers proposed a spectral analysis, which gives the inverse Laplace transform of the transient.[45] Due to the complexity of the transient, this transformation can only be done numerically, and it requires estimated minimum and maximum emission rates for calculation.[46] For the DLPTS transients with the aforementioned three stages, the inverse Laplace transformation requires a very large range of emission rates and computational results are not stable. Although one can remove fast components by successive subtraction of the transient,[47] however, by doing so it is very difficult to keep the slow transient unchanged, especially for multiple-level cases such as encountered in SI-GaAs DLPTS. Due to the ill-posed nature of the inverse Laplace solution, our calculations based on the FTIKREG (Ref. 46) program indicate that the inverse Laplace solution is not unique and is extremely sensitive to baseline subtraction. Therefore, our combined-modality approach clearly shows that lock-in amplifier emission-level analysis combining thermal and pulse-rate spectra is the optimal defect-level diagnostic method for DLPTS.

Although the time-domain transient suffers from the low energetic resolution, it presents the raw signal entering the detector and provides a clear validation of DLPTS signal generation theory. As mentioned earlier (Sec. VI A), DLTS measurements could be either $n(t)$ sensitive or $n_T(t)$ sensitive and both approaches reveal peaks in the thermal spectra. Since the probe light in DLPTS detects both $n(t)$ and $n_T(t)$, it is difficult to identify the main contributing component merely from the thermal or pulse-rate spectrum. This issue, however, can be easily resolved by examining the magnitude of the slow recovery component in the transient. Due to the more dominant band-to-band recombination, the slow recovery component in $n(t)$ transient is usually very small. As shown in the general solutions, Eqs. (17) and (18), the magnitude of the slow recovery component in $n(t)$ is determined by $\Sigma_{j=1}^{m}[e_{nj}(E_j)/\tau^{-1}-e_{nj}(E_j)]n_{Tj}(t_p)$, while in the $n_T(t)$ transient, it is controlled by $n_{Tj}(t_p)$. Since $\tau^{-1} \gg e_{nj}(E_j)$, $\Sigma_{j=1}^{m}[e_{nj}(E_j)/\tau^{-1}-e_{nj}(E_j)]n_{Tj}(t_p)$ can be written as $\Sigma_{j=1}^{m}[e_{nj}(E_j)/\tau^{-1}]n_{Tj}(t_p)$, which is much smaller than $\Sigma_{j=1}^{m}n_{Tj}(t_p)$. Figure 13 shows the $n(t)$ and $n_T(t)$ transients from a single defect level (EL3 level). The slow recovery in $n(t)$ transient can only be seen after being magnified for 20 000 times. For this reason, transients in Fig. 12 clearly demonstrate that the DLPTS signal mainly originates in the absorption of $n_T(t)$. The transient evaluation of the relative contributions from $n(t)$ and $n_T(t)$ absorption will be ex-

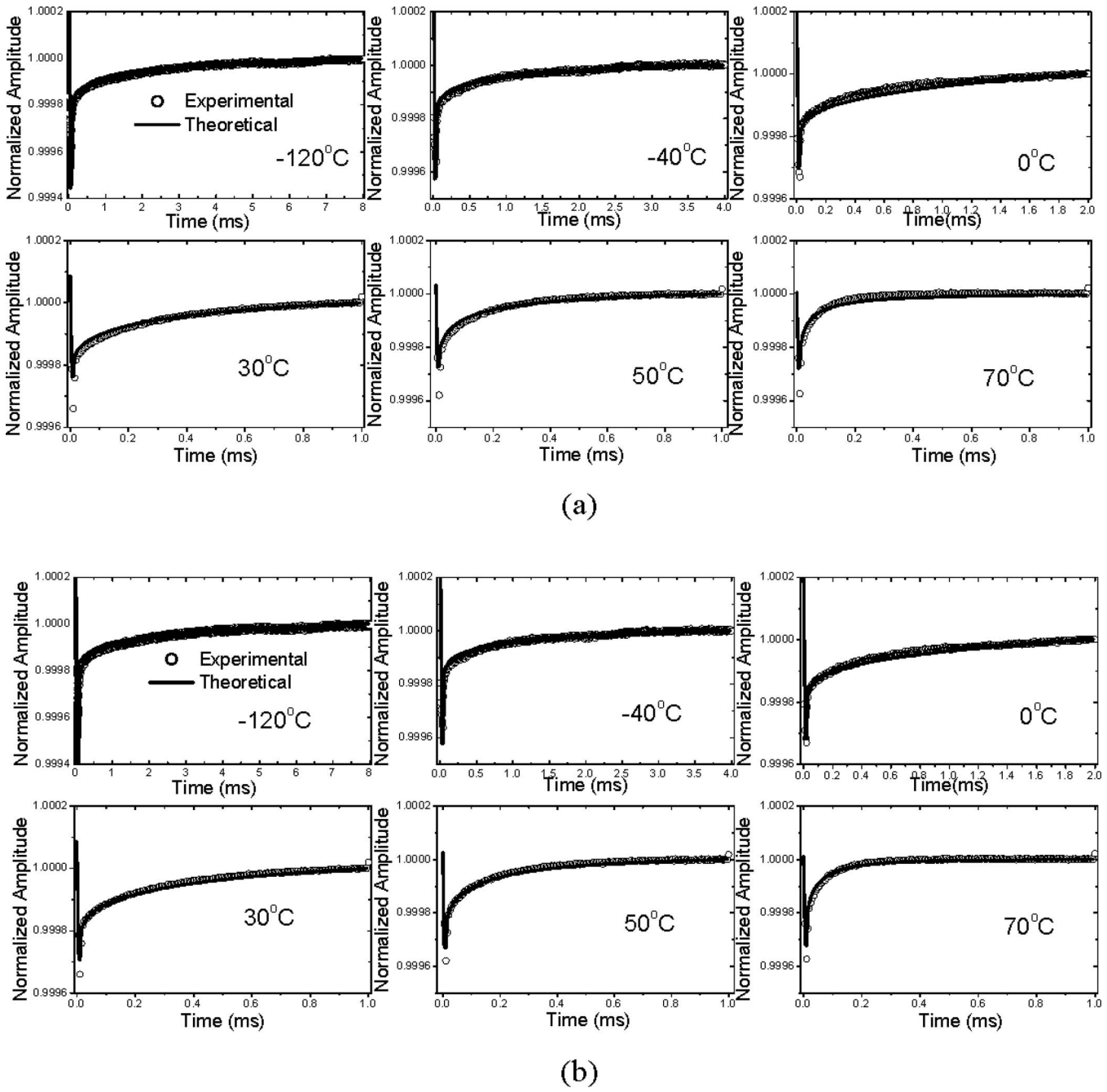

FIG. 12. Experimental and theoretical time-scanned DLPTS transients at various temperatures. (a) Theory with Gaussian activation energy broadening. (b) Theory with stretched exponential β_2 broadening.

tremely important when DLPTS measurements are performed on semiconductors with unknown absorption coefficient at the probing wavelength.

VII. CONCLUSIONS

In comparison with all the DLPTS modalities, the temperature-scanned spectrum is the easiest to interpret theoretically, since the data have already been analyzed by the lock-in amplifier and the amplitude spectrum is shown to be a superposition of various defect levels. This approach is also most widely used with DLTS based measurements, such as PITS.[34] However, in those studies only magnitude spectra are analyzed without regard to pulse repetition rate or phase. Our research shows that the phase spectrum contains additional information not easily garnered in the amplitude spectrum, like the HL3 and EL2 levels in SI-GaAs. The combination of temperature and pulse-rate DLPTS enhances the specificity of the DLPTS technique to trapped carrier energetics and kinetics. Even with excellent theoretical agreement with the amplitude spectrum, the theoretical phase spectrum may still exhibit discrepancies at high frequencies, which indicate additional kinetics may need to be considered. The pulse-rate-scanned spectrum yields a single peak in the measured pulse-rate (frequency) range. As expected, the pulse-rate scan requires a much broader bandwidth in order to cover all defect states accessible to photothermal temperature scans. Un-

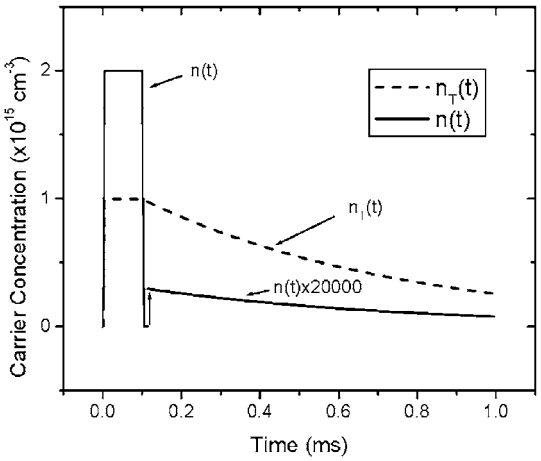

FIG. 13. Theoretical $n(t)$ and $n_T(t)$ transients from a single defect (EL3) level. Simulations are based on the nonbroadened theory.

like the peaks in the temperature amplitude spectrum, the pulse-rate peak position is found to be sensitive to the optical power of the excitation laser. Combined with the photothermal temperature phase spectrum, DLPTS may provide a unique tool for detailed studies of photocarrier excitation mechanisms as a function of pulse repetition frequency. DLPTS time-domain transients represent the raw signal from the detector and provide a clear illustration of DLPTS kinetics. Although transients suffer from low trap-level resolution, they are can be used to determine the relative contributions of $n(t)$ and $n_T(t)$ absorptions, which are essential for wider applications of DLPTS technique.

With regard to the physical implications of the DLPTS broadening mechanisms, a hierarchical carrier emission theory was developed capable of generating good fits to DLPTS temperature spectra, pulse-rate scans, and photothermal transients. The theory provides a possible explanation for the stretched exponential behavior commonly observed in DLTS measurements and also confirms the existence of electron-to-electron constrained kinetics from trapped states in SI-GaAs. When compared with the more widely used Gaussian distribution theory, the hierarchical theory gives similar broadening on experimental data of all DLPTS modalities. This theory allows a wider application of stretched-exponential characterization in semiconductor systems and also provides an energetic broadening parameter ΔE as in the Gaussian distribution theory. For equivalent broadening effects, the ratio $\delta E/\Delta E=1.5$ for defect states with higher activation energies (higher resonance temperatures), while it decreases, and is close to 1 for defects with lower activation energies (lower resonance temperatures). The existence of a relationship between the Gaussian and stretched exponential-induced trap-state energy broadening mechanisms demonstrates a statistical relation between the emission kinetics of the trapped electron system and their random energetic distribution in the trap microstate manifold, the first reported manifestation of the temperature-dependent ergodic nature of trap (defect) state kinetics in SI-GaAs. The evidence of a changing $\delta E/\Delta E$ ratio at low temperatures also indicates this statistical relation depends on degrees of disorder in systems. The ergodic nature of the emission process is supported by all three DLPTS modalities.

ACKNOWLEDGMENTS

The authors are grateful to the Natural Sciences and Engineering Research Council of Canada (NSERC) for Discovery and Research Tools and Instruments (RTI) grants to A.M., which made this research possible. The collaboration of Dr. T. Ikari and Dr. Fukuyama in providing the PPT spectra of our SI-GaAs samples is gratefully acknowledged and valuable discussion on the PPT spectra is deeply appreciated.

[1]D. V. Lang, J. Appl. Phys. **45**, 3023 (1974).
[2]M. J. S. P. Brasil and P. Motisuke, J. Appl. Phys. **68**, 3370 (1990).
[3]J. C. Abele, R. E. Kremer, and J. S. Blakemore, J. Appl. Phys. **62**, 2432 (1987).
[4]L. E. Benatar, D. Redfield, and R. H. Bube, J. Appl. Phys. **73**, 8659 (1993).
[5]P. K. Giri and Y. N. Mohapatra, J. Appl. Phys. **78**, 262 (1995).
[6]A. Das, V. A. Singh, and D. V. Lang, Semicond. Sci. Technol. **3**, 1177 (1988).
[7]Ch. Hardalov, I. Yanchev, K. Germanova, Tzv. Ivanov, L. Samurkova, K. Kirov, and A. Nigohosian, J. Appl. Phys. **71**, 2270 (1992).
[8]J. Xia and A. Mandelis, Appl. Phys. Lett. **90**, 062119 (2007).
[9]A. Mandelis and J. Xia, J. Appl. Phys. **103**, 043704 (2008).
[10]P. Omling, L. Samuelson, and H. G. Grimmeiss, J. Appl. Phys. **54**, 5117 (1983).
[11]C. Kisielowski and E. R. Weber, Phys. Rev. B **44**, 1600 (1991).
[12]L. C. Kimerling and J. R. Patel, Appl. Phys. Lett. **34**, 73 (1979).
[13]K. Sato, K. Tanaka, J. Yoshino, Y. Okamoto, J. Morimoto, and T. Miyakawa, Mater. Sci. Forum **196-201**, 267 (1995).
[14]A. Ginoudi, E. C. Paloura, and N. Frangis, J. Appl. Phys. **75**, 2980 (1994).
[15]S. Orsila, A. Tukiainen, P. Uusimaa, J. Dekker, T. Leinonen, and M. Pessa, J. Cryst. Growth **227-228**, 249 (2001).
[16]A. A. Teate and N. C. Halder, J. Appl. Phys. **70**, 1455 (1991).
[17]L. Papadimitriou, Solid-State Electron. **36**, 431 (1993).
[18]D. A. Batovski and Ch. M. Hardalov, J. Appl. Phys. **74**, 291 (1993).
[19]G. Williams and D. C. Watts, Trans. Faraday Soc. **66**, 80 (1970).
[20]A. K. Jonscher, Nature (London) **267**, 673 (1977).
[21]R. H. Boyd and C. H. Porter, J. Polym. Sci. A **2**, 647 (1972).
[22]H. Yonekura, T. Arai, J. Morimoto, and T. Miyakawa, Jpn. J. Appl. Phys., Part 2 **29**, L101 (1990).
[23]L. E. Benatar, D. Redfield, and R. H. Bube, J. Appl. Phys. **73**, 8659 (1993).
[24]E. W. Montroll and J. T. Bendler, J. Stat. Phys. **34**, 129 (1984).
[25]K. Kim and A. J. Epstein, Appl. Phys. Lett. **67**, 2786 (1995).
[26]P. M. Mooney, in *Degradation Mechanisms in III-V Compound Semiconductor Devices and structures*, edited by V. Swaminathan, S. J. Pearton, and M. O. Manasreh (Materials Research Society, Pittsburgh, 1990), Vol. 184.
[27]A. Chantre, G. Vincent, and D. Bois, Phys. Rev. B **23**, 5335 (1981).
[28]R. G. Palmer, D. L. Stein, E. Abrahams, and P. W. Anderson, Phys. Rev. Lett. **53**, 958 (1984).
[29]S. M. Sze, in *Physics of Semiconductor Devices*, 2nd ed.(Wiley-Interscience, New York, 1981), Chap. 2.
[30]R. V. Chamberlin, G. Mozurkewich, and R. Orbach, Phys. Rev. Lett. **52**, 867 (1984).
[31]F. Mezei and A. P. Murani, J. Magn. Magn. Mater. **14**, 211 (1979).
[32]A. Mandelis, J. Batista, and D. Shaughnessy, Phys. Rev. B **67**, 205208 (2003).
[33]G. Antonioli, D. Bianchi, and P. Franzosi, Phys. Status Solidi B **106**, 79 (1981).
[34]P. Kaminski and R. Kozlowski, Mater. Sci. Eng., B **91-92**, 398 (2002).
[35]J. C. Bourgoin, H. J. von Bardeleben, and D. Stievenard, J. Appl. Phys. **64**, R65 (1988).
[36]K. Petersen, *Ergodic Theory, Cambridge Studies in Advanced Mathematics* (Cambridge University Press, Cambridge, 1990).
[37]L. Pavesi and M. Ceschini, Phys. Rev. B **48**, 17625 (1993).
[38]J. C. Phillips, Phys. Rev. B **52**, R8637 (1995).

[39]J.-P. Eckmann and I. Procaccia, Phys. Rev. E **78**, 011503 (2008).
[40]T. Ikari, A. Fukuyama, and A. Goto, Miyazaki University, Japan, private communication (December 2006).
[41]A. Fukuyama, A. Memon, K. Sakai, Y. Akashi, and T. Ikari, J. Appl. Phys. **89**, 1751 (2001).
[42]D. C. Look, in *Semiconductors and Semimetals*, edited by R. K. Willardson and A. C. Beer (Academic, New York, 1983), Vol. 19, p. 113.
[43]G. M. Martin, Appl. Phys. Lett. **39**, 747 (1981).
[44]P. M. Henry, J. M. Meese, J. W. Farmer, and C. D. Lamp, J. Appl. Phys. **57**, 628 (1985).
[45]L. Dobaczewski, A. R. Peaker, and K. Bonde Nielsen, J. Appl. Phys. **96**, 4689 (2004).
[46]J. Weese, Comput. Phys. Commun. **69**, 99 (1992).
[47]J. C. Abele, R. E. Kremer, and J. S. Blakemore, J. Appl. Phys. **62**, 2432 (1987).